Colors of the daytime overcast sky

Raymond L. Lee, Jr. and Javier Hernández-Andrés

Time-series measurements of daylight (skylight plus direct sunlight) spectra beneath overcast skies reveal an unexpectedly wide gamut of pastel colors. Analyses of these spectra indicate that at visible wavelengths, overcasts are far from spectrally neutral transmitters of the daylight incident on their tops. Colorimetric analyses show that overcasts make daylight bluer and that the amount of bluing increases with cloud optical depth. Simulations using the radiative-transfer model MODTRAN4 help explain the observed bluing: multiple scattering within optically thick clouds greatly enhances spectrally selective absorption by water droplets. However, other factors affecting overcast colors seen from below range from minimal (cloud-top heights) to moot (surface colors).

OCIS codes: 010.1290, 290.1090, 330.1710, 330.1730.

1. Introduction

In the extended family of atmospheric optical phenomena, overcast skies are surely the poor relations. Lacking the distinct, vivid colors of such prodigals as parhelia and rainbows, overcasts have prompted relatively little spectral research outside the ultraviolet and infrared, where their radiative-transfer properties are important.[1–3] With relatively few exceptions,[4–6] even those researchers who do analyze overcasts at visible wavelengths are interested chiefly in explaining the clouds' spectral properties independent of human perception.[3,7–9] And although the CIE has recommended a particular model for the *angular* distribution of overcast luminances,[10] it is far less specific about the *spectral* distribution of overcast radiances or irradiances, instead indicating that overcast spectra are simple variants on its standard daylight illuminant D_{65}.[11]

This relative scientific neglect of overcast color is paired with popular disdain: in everyday parlance, overcasts are the dark, dreary, and dull-colored alternatives to visually pleasing clear or partly cloudy skies. Implicit in such language is the plausible (but incorrect) assumption that overcasts are spectrally neutral transmitters of the daylight (skylight plus direct sunlight) incident on them.[12] Yet our research shows that overcast colors are seldom as gray as we might imagine, and explaining why overcasts are spectrally selective yields useful insights into radiative transfer in clouds.

2. Measured Chromaticities of Daytime Overcasts

Because "overcast" has slightly different meanings in different contexts, we start by defining the term. In our work, an overcast must meet two criteria: (1) no clear sky can be visible anywhere and (2) cloud cover must be sufficiently optically thick that any cast shadows are indistinct. Unlike some definitions of overcast,[13] ours includes surface fog that obscures (or perhaps is) the sky. We restrict ourselves here to daytime overcasts when unrefracted Sun elevation $h_0 \geq 5°$ because overcast color behaves quite differently at lower h_0. Although most of our overcasts were formed by thick stratus (St) or stratocumulus (Sc) clouds, we also measured altostratus overcasts through which the Sun's disk was faintly visible. To protect our instruments, we measured mostly nonprecipitating overcasts. With care, however, we also were able to acquire some data in drizzle, light rain, and snow. What kinds of chromaticity gamuts do such overcasts produce?

Figure 1 shows part of the CIE 1976 uniform-chromaticity-scale (UCS) diagram,[14] within which we plot temporal chromaticity trends produced by two typical overcasts. We generate such curves by measuring overcast spectra every 30 s and then connecting in sequence the individual u', v' chromaticity coordinates calculated from each spectrum. Included as colorimetric landmarks in Fig. 1 are part of the

R. L. Lee (raylee@usna.edu) is with the Mathematics and Science Division, United States Naval Academy, Annapolis, Maryland 21402. J. Hernández-Andrés is with Departamento de Optica, Facultad de Ciencias, Universidad de Granada, Granada 18071, Spain.

Received 13 December 2004; revised manuscript received 12 May 2005; accepted 19 May 2005.

0003-6935/05/275712-11$15.00/0

Report Documentation Page

Form Approved
OMB No. 0704-0188

1. REPORT DATE	2. REPORT TYPE	3. DATES COVERED
12 MAY 2005		**00-00-2005 to 00-00-2005**

4. TITLE AND SUBTITLE	5a. CONTRACT NUMBER
Colors of the daytime overcast sky	5b. GRANT NUMBER
	5c. PROGRAM ELEMENT NUMBER
6. AUTHOR(S)	5d. PROJECT NUMBER
	5e. TASK NUMBER
	5f. WORK UNIT NUMBER
7. PERFORMING ORGANIZATION NAME(S) AND ADDRESS(ES) **United States Naval Academy (USNA),Mathematics & Science Department,Annapolis,MD,21402**	8. PERFORMING ORGANIZATION REPORT NUMBER
9. SPONSORING/MONITORING AGENCY NAME(S) AND ADDRESS(ES)	10. SPONSOR/MONITOR'S ACRONYM(S)
	11. SPONSOR/MONITOR'S REPORT NUMBER(S)

12. DISTRIBUTION/AVAILABILITY STATEMENT
Approved for public release; distribution unlimited

13. SUPPLEMENTARY NOTES

14. ABSTRACT

15. SUBJECT TERMS

16. SECURITY CLASSIFICATION OF:			17. LIMITATION OF ABSTRACT	18. NUMBER OF PAGES	19a. NAME OF RESPONSIBLE PERSON
a. REPORT **unclassified**	b. ABSTRACT **unclassified**	c. THIS PAGE **unclassified**	**Same as Report (SAR)**	**11**	

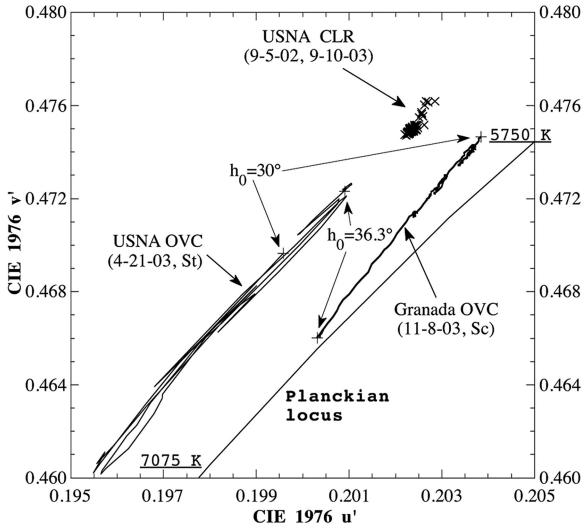

Fig. 1. Portion of the CIE 1976 UCS diagram, showing temporal trends in stratus (St) and stratocumulus (Sc) overcast chromaticities measured at the U.S. Naval Academy in Annapolis, Maryland (USNA) on 4-21-2003 and at the University of Granada in Granada, Spain on 11-8-03. Chromaticities are calculated from horizontal spectral irradiances E_λ. For comparison, we also show chromaticities from two cloudless days at USNA (9-5-02, 9-10-03). On each day, unrefracted Sun elevation h_0 ranges from 30.0°–36.3°.

Planckian locus and its corresponding color-temperature limits. Figure 1's observing sites are the University of Granada at Granada, Spain, and the U.S. Naval Academy (USNA) at Annapolis, Maryland. We selected the Fig. 1 curves from our time series of >9100 radiance and irradiance spectra measured during 40 overcasts at USNA and Granada, as well as at two rural sites near Owings, Maryland, and Marion Center, Pennsylvania. Table 1 gives details of the sites' locations; we made all observations at ground or rooftop level.

Table 1. Geographic Details of Our Measurement Sites

Site Name	Latitude	Longitude	Elevation (m)
Granada, Spain	37° 11′ N	3° 35′ W	680
Marion Center, Pa.	40° 49′ N	79° 5′ W	451
Owings, Md.	38° 41′ N	76° 35′ W	15
USNA, Md.	38° 59′ N	76° 29′ W	18

Our instruments are two Photo Research PR-650 spectroradiometers, with which we measure either zenith spectral radiances L_λ or horizontal spectral irradiances E_λ at visible wavelengths λ. Both radiometers have spectral ranges of 380–780 nm and a step size of 4 nm.[15] Zenith radiances are measured across a 1° field of view (FOV) by using a telescopic lens on the PR-650, and hemispheric irradiances are measured using a nominally cosine-corrected diffuser (FOV = 2π sr). We aimed the radiometer and then locked it on a tripod before each measurement session. Figure 1's chromaticities, are calculated from horizontal E_λ and show only parts of such sessions: each curve spans the period when $30° < h_0 < 36.3°$. Figure 1 also shows the range of clear daylight chromaticities (abbreviated CLR and plotted using ×'s) measured on two clear days for the same h_0 interval. The conventional meteorological abbreviations "OVC" and "CLR" in Fig. 1 indicate overcast and clear, respectively.

Several colorimetric features are noteworthy in Fig. 1. First, its chromaticity gamut for clear daylight is much less than for its two stratus and stratocumulus overcasts. Using the normalized colorimetric gamut $\hat{g}$,[16] Fig. 1's two overcast gamuts are 7.0 and 13.8 times larger than the combined clear-sky gamut (see Table 2). Thus an overcast's colors are only partly determined by the daylight color that illuminates its cloud tops. Second, Fig. 1 shows that overcasts are usually bluer (i.e., have higher color temperature) than clear daylight,[6] although this enhanced blueness can vary significantly from minute to minute. If our claim that overcasts are bluer than clear daylight seems puzzling, recall that Fig. 1 is based on *hemispheric* E_λ rather than on narrow-FOV L_λ, and thus its clear-sky cases are dominated by direct sunlight. During the day, the clear sky's blue is indeed much purer than that of the bluest overcast. Third, unlike

Table 2. Mean Overcast Chromaticities and Chromaticity Gamuts

Figure	Dates	E_λ or L_λ[a]	h_0 Interval (°)	Mean u'	Mean v'	$\hat{g}$
1	9-5-02, 9-10-03	E_λ	30.0–36.3	0.20239	0.47507	0.0011029
1	11-8-03	E_λ	30.0–36.3	0.20291	0.47238	0.0076751
1	4-21-03	E_λ	30.0–36.3	0.19855	0.46716	0.015191
3	4-17-03	L_λ	46.6–60.3	0.20035	0.46935	0.0018261
3	5-22-03	L_λ	46.6–60.3	0.19707	0.46780	0.0013432
3	6-16-03	L_λ	46.6–60.3	0.19901	0.46901	0.0041030
17	10-12-02	E_λ	5.0–12.3	0.19893	0.47027	0.014782
17	11-15-03	E_λ	5.0–12.3	0.20014	0.46677	0.0070159
19	2-6-03	L_λ	14.4–20.5	0.19757	0.46132	0.0086214
19	2-17-03	L_λ	14.4–20.5	0.19824	0.46523	0.015537
20	1-1-03	L_λ	12.3–20.2	0.19690	0.46519	0.013589
20	1-2-03	L_λ	12.3–20.2	0.19709	0.46276	0.0066675
20	1-16-03	L_λ	12.3–20.2	0.19868	0.46423	0.0082847

[a]Denotes whether chromaticities in a given figure are calculated from spectral horizontal irradiances E_λ or zenith radiances L_λ.

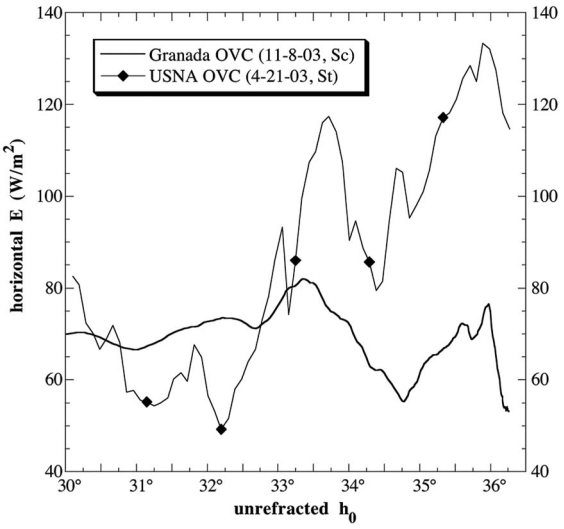

Fig. 2. Spectrally integrated horizontal irradiances E versus h_0 for Fig. 1's two overcasts. Integrals are calculated from 380–780 nm in 4 nm steps.

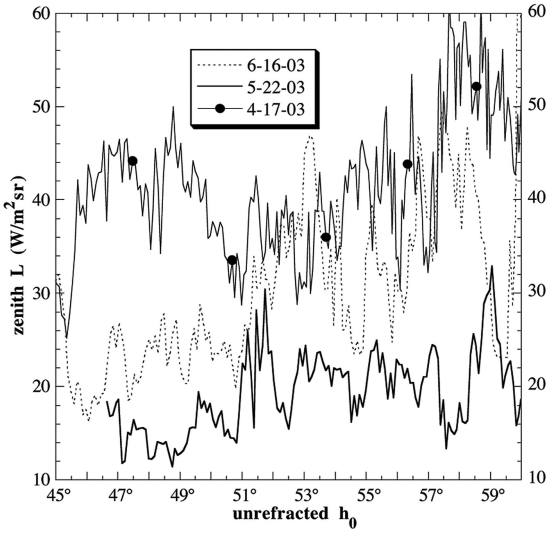

Fig. 4. Spectrally integrated zenith radiances L versus h_0 for Fig. 3's three stratus overcasts at Owings. The spectroradiometer's measurement FOV is 1°, and integrals are calculated from 380–780 nm in 4 nm steps.

the often smooth chromaticity curves produced by clear twilights,[17] daytime overcast curves tend to be erratic, with colors shifting from one measurement to the next in response to clouds' fluctuating E_λ and optical depth τ (see Fig. 2's time series of integrated E). Although such daylight color shifts are detectable in principle,[18] in practice most go unnoticed.

Even if cloud type does not change, the color gamuts of overcasts on different days may differ perceptibly for the same h_0 interval. Figure 3 shows chromaticities from zenith L_λ for three different stratus overcasts at the Owings site when $46.6° < h_0 < 60.3°$. Because measured overcast chromaticities seldom change linearly, beginning in Fig. 3 we usually omit line segments between temporally adjacent colors. This plotting convention makes the details of our chromaticity gamuts somewhat clearer. Like all our daytime overcast measurements (i.e., those taken when $h_0 \geq 5°$), Fig. 3's chromaticities are to the left of the Planckian locus. Moreover, these three overcasts have more-or-less distinct chromaticity clusters that differ from one another on the CIE diagram by ~1 MacAdam just-noticeable difference (or JND; 1 JND is the horizontal line at upper right in Fig. 3).[19] In other words, if typical observers simultaneously compared Fig. 3's clusters of overcast colors, most could *just* distinguish among them. But because we do not actually have this perceptual luxury, we seldom notice such small color shifts between different overcasts.

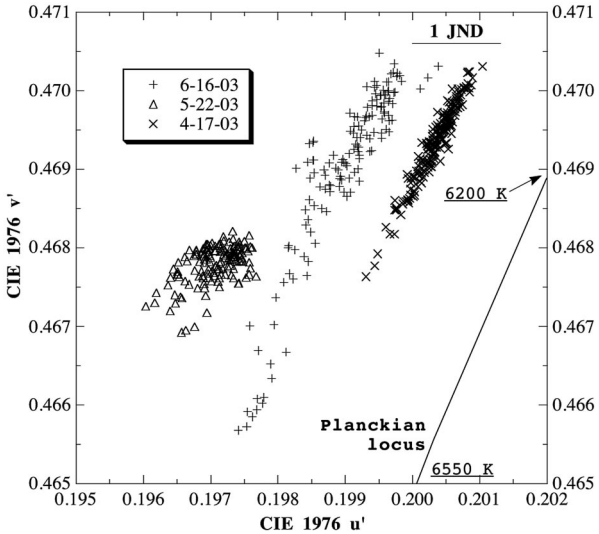

Fig. 3. Scatterplot of overcast u', v' chromaticities calculated from zenith spectral radiances L_λ at Owings, Maryland, during stratus overcasts on 4-17-03, 5-22-03, and 6-16-03; h_0 ranges from 46.6°–60.3°. The length of the bar labeled "1 JND" equals the local MacAdam just-noticeable difference in chromaticity.

Figure 4, which shows L time series for Fig. 3's chromaticities, helps to explain differences in overcast color. Although all three overcasts in Figs. 3 and 4 consisted of stratus, their appearance ranged from distinctly variegated (4-17-03) to almost featureless (5-22-03). As clouds moved across the radiometer's zenith FOV, the resulting changes in τ caused the fluctuations in both spectral L_λ and integrated L seen in Figs. 3 and 4. Because the 5-22-03 overcast had the most spatially uniform τ, it has the smallest L dynamic range (or ratio of maximum to minimum L) and smallest $\hat{g}$. Conversely, the overcast with the largest L dynamic range (6-16-03; see Fig. 4's dashed curve) has the largest $\hat{g}$. Thus increased variability in overcast τ *tends* to make $\hat{g}$ larger, and it also seems to change the colorimetric position of that gamut. In particular, the darkest overcast in Fig. 4 (5-22-03) is also the bluest in Fig. 3. We see this relationship directly in Fig. 5, where the lower-E (and thus higher-τ) right half of the fisheye image is distinctly bluer than the higher-E left half. Because we fixed

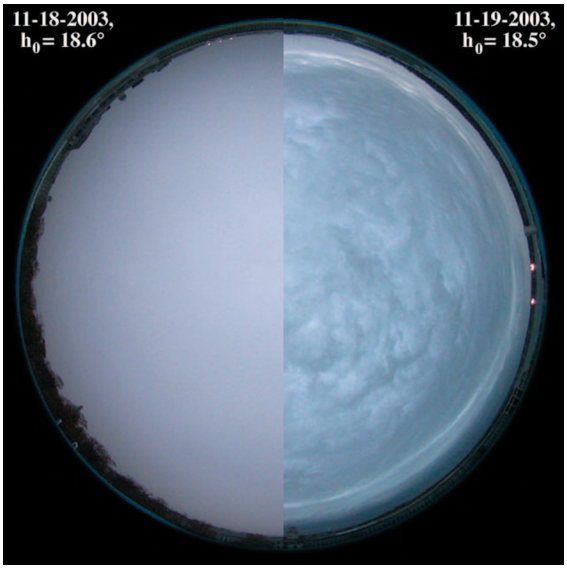

Fig. 5. Composite fisheye image of a bright stratus overcast (left half, $E = 24.3\ \mathrm{W\ m^{-2}}$) and a much darker stratocumulus overcast (right half, $E \sim 3.6\ \mathrm{W\ m^{-2}}$) at USNA on 11-18-03 and 11-19-03, respectively. Note that the darker overcast is distinctly bluer. Although exposures differ, in both original photographs the digital camera's white-balance setting was the same and $h_0 \sim 18.5°$.

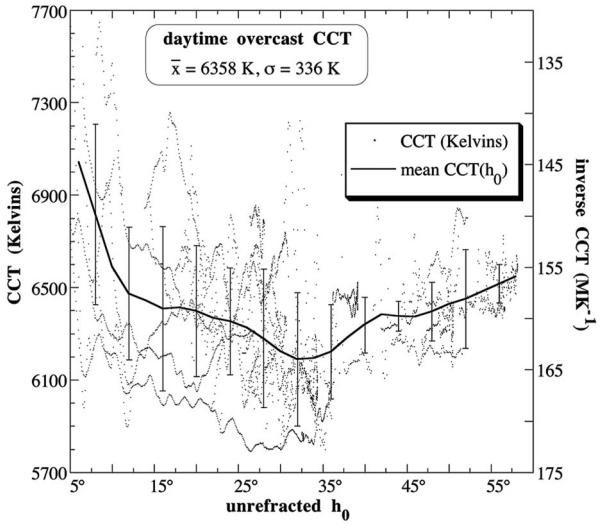

Fig. 6. Correlated color temperature (CCT) in Kelvins versus h_0 for all 4278 of our horizontal E_λ spectra for overcasts; individual CCTs are plotted as dots. The right-hand ordinate gives equivalent values of inverse CCT, which is measured in inverse mega-Kelvins (10^6/CCT; inverse CCT unit is $\mathrm{MK^{-1}}$). The mean CCT curve is calculated using bins that are 2° wide in h_0, and each error bar spans 2 standard deviations σ at the given h_0.

the digital camera's white balance when we took Fig. 5's photographs, their color shift is real and not an electronic artifact. Optical explanations for these overcast color phenomena appear in Section 4.

3. Correlated Color Temperatures of Daytime Overcasts

Correlated color temperature (CCT) has long been used as an approximate, convenient alternative to chromaticity coordinates near the Planckian locus.[20] Because CCT reduces two-dimensional color data (u', v') to one dimension, CCT's convenience comes at the cost of some colorimetric ambiguity. For example, although a 6000-Kelvin CCT can be on either side of the Planckian locus,[21] all our measurements of daytime overcast CCTs place them on its left (or greenish) side. In Fig. 6, we show how overcast CCT varies with h_0 for nearly half our 9100 daytime spectra. These are the E_λ spectra measured from the entire sky hemisphere; i.e., they are spectra of overcast daylight as opposed to skylight. Although cloud spectral optical depth τ_λ and the underlying surface's spectral reflectance r_λ also influence overcast CCT,[4] h_0 partly determines the daylight spectrum incident on an overcast's top. In turn, this daylight spectrum affects overcast color as seen from the ground.

Because the incident illumination is only one of several factors governing overcast color, h_0 and CCT are weakly correlated in Fig. 6. Yet as in our earlier work,[6] mean overcast CCT in Fig. 6 clearly has a local minimum (i.e., is reddest) when $30° < h_0 < 35°$. Although Fig. 6's CCT variance might eliminate this local minimum, the distinct trend in mean CCT at nearby h_0 suggests otherwise. If indeed this CCT minimum is real, we lack a ready explanation for it: our measurements indicate that clear daylight at the surface (i.e., combined skylight and direct sunlight) usually does not begin to redden until $20° < h_0 < 25°$. Furthermore, we cannot blame the overcast itself for this reddening. As demonstrated in Section 4, diffuse transmission through optically thick clouds makes the transmitted light slightly bluer, not redder.

The mean and median overcast CCTs in Fig. 6 are 6358 K and 6341 K, respectively. Although these values are ~375 K larger than the mean overcast CCTs that we reported earlier,[6] this is unlikely to be perceptually significant, especially given that the overall standard deviation $\sigma = 336$ K is nearly as large as the CCT difference. In fact, our new mean and median CCT are closer to the 6500 K overcast white-balance setting suggested by some digital camera manufacturers.[22] The extreme daytime CCTs are 9316 K (bluest) and 5799 K (least blue), and we plot the corresponding E_λ spectra in Fig. 7. The high-CCT spectrum occurred when $h_0 = 5.0°$, our self-imposed lower limit on daytime h_0. That the maximum CCT occurred at the lowest h_0 is not surprising, because even though direct sunlight atop the overcast is reddened then, the combined effects of atmospheric extinction and the cosine law mean that it contributes relatively little to horizontal E_λ.[17] Instead, bluish skylight dominates illumination both above and below the clouds.

Figure 8's histogram gives the distribution of all daytime overcast color temperatures, here shown as inverse CCTs.[6] The unit of inverse CCT is the reciprocal mega-Kelvin (10^6/CCT), denoted by the symbol $\mathrm{MK^{-1}}$ (originally called the "mired").[23] Reciprocal mega-Kelvins produce a uniform scale that better

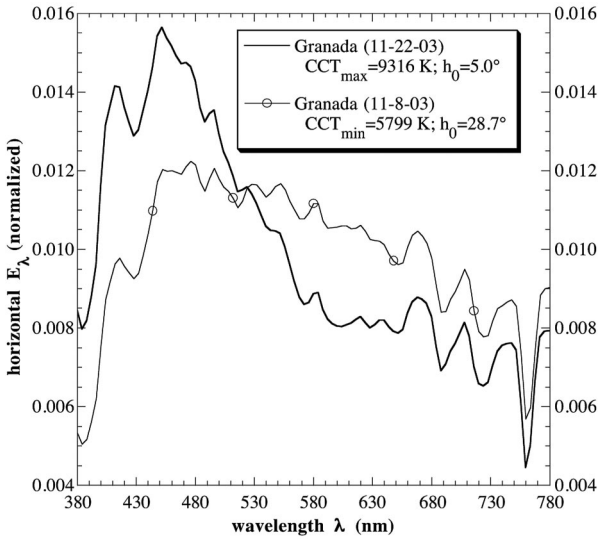

Fig. 7. Normalized horizontal irradiances E_λ for the two daytime spectra having the maximum and minimum CCTs in our data (9316 K and 5799 K). These spectra yield our colorimetric extremes in daytime overcasts. Each original spectrum is normalized by its sum; to convert normalized to absolute irradiances, multiply the 11-22-03 E_λ by 0.814 W m^{-2} nm^{-1} and the 11-8-03 E_λ by 16.3 W m^{-2} nm^{-1}.

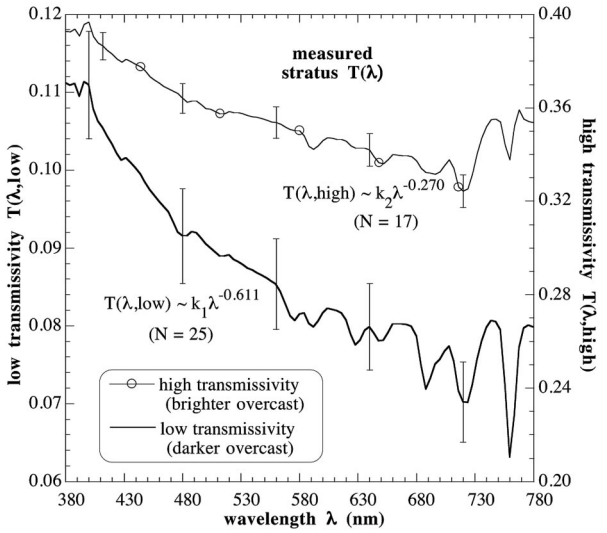

Fig. 9. Mean $T(\lambda)$ transmission spectra for E_λ spectra measured at USNA during stratus overcasts on 4-4, 4-8, and 4-21-03; h_0 ranges from 40.1°–57.7°. $N = 25$ and $N = 17$ irradiance spectra were used to calculate the mean $T(\lambda, \text{low})$ and $T(\lambda, \text{high})$ spectra, respectively. Each error bar spans 2σ at the given wavelength. Best-fit equations are for the interval $400 \le \lambda \le 680$ nm, with proportionality constants $k_1 = 4.077$ and $k_2 = 1.946$.

describes human color sensitivity than does CCT itself. On this inverse CCT scale, our overcast spectra have a mean = 157.7 MK^{-1}, σ = 7.79 MK^{-1}, and a modal interval of 154–156 MK^{-1}. Clearly Fig. 8 is skewed left toward smaller inverse CCT, and this is caused by a relatively few high-CCT overcasts seen at low h_0 (see Fig. 6's left side).

4. Blue Clouds and Overcast Transmission Spectra

A fundamental problem in analyzing overcast colors is that the continual changes in cloud E and L (see Figs. 2, 4) further complicate an already complex optical system. We take two different tacks in addressing this problem: (1) averaging measured spectra over a small range of h_0 and (2) modeling the effects of individual parameters on overcast colors.

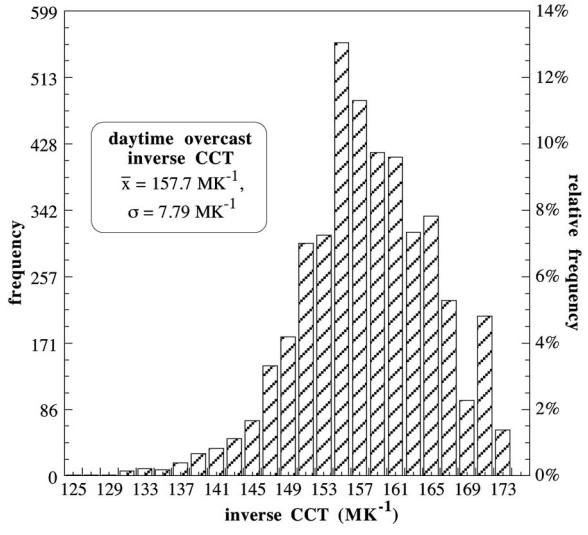

Fig. 8. Histogram of inverse CCT for our 4278 overcast E_λ spectra. The modal interval is 154–156 MK^{-1}, and each bin is 2 MK^{-1} wide.

We start by defining an overcast's spectral transmissivity $T(\lambda)$, where

$$T(\lambda) = \frac{E(\lambda, \text{OVC})}{E(\lambda, \text{CLR})} \tag{1}$$

is the ratio of an overcast's downwelling spectral irradiances $E(\lambda, \text{OVC})$ to those of some average $E(\lambda, \text{CLR})$ for clear daylight at the same h_0. This last qualification is needed because both $E(\lambda, \text{OVC})$ and $E(\lambda, \text{CLR})$ are functions of h_0. Here we average E_λ spectra from the clear afternoons of 9-5-02 and 9-10-03 at USNA (see Fig. 1). In radiative-transfer models, an overcast's T usually is usually defined as the ratio of downwelling irradiance at cloud bottom to that at cloud top (i.e., incident daylight). However, our ground-based measurement of T is nearly equivalent because many overcast cloud tops and bottoms are fairly close to the ground.[24]

Figure 9 shows two stratus $T(\lambda)$ spectra, each averaged over N overcast irradiance spectra with either relatively low T ($N = 25$) or high T ($N = 17$). The original overcast E_λ spectra were acquired over a restricted h_0 range on several different days. To show more spectral detail, we draw the two $T(\lambda)$ spectra with different ordinate scales, and these scales preserve the relative slopes of the two curves. Figure 9 provides unambiguous spectral evidence that both low-T (or darker) and high-T (or brighter) overcasts shift incident daylight toward the blue, as indicated

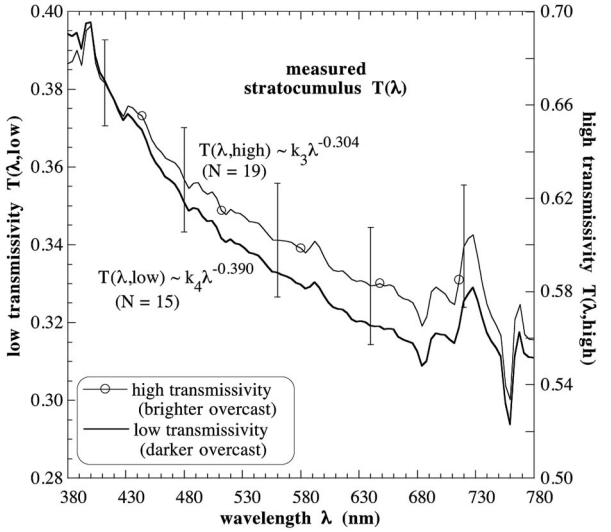

Fig. 10. Mean $T(\lambda)$ spectra for E_λ spectra measured at USNA during a stratocumulus overcast on 3-19-03; h_0 ranges from 41.9°–50.5°. $N = 15$ and $N = 19$ irradiance spectra were used to calculate the mean low- and high-transmissivity $T(\lambda)$ spectra, respectively. Each error bar spans 2σ at the given wavelength, and for clarity we show bars only for the $T(\lambda, \text{high})$ curve. Best-fit equations are for the interval $400 \le \lambda \le 680$ nm, with proportionality constants $k_3 = 4.136$ and $k_4 = 3.943$.

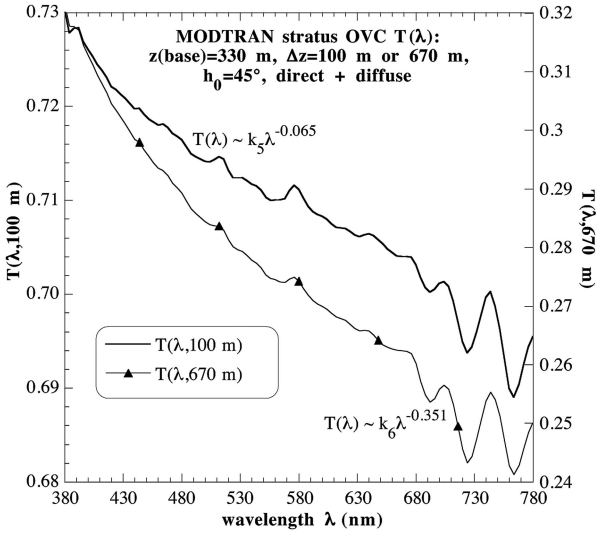

Fig. 11. MODTRAN4 simulated $T(\lambda)$ spectra for the model's default stratus overcast when its clouds are 100 m or 670 m thick. In both cases, $h_0 = 45°$, and cloud base is 330 m above the surface. For the thicker overcast, we calculate $T(\lambda)$ using combined direct-beam and diffuse irradiances at the surface, but we switch to irradiances calculated at cloud top and bottom for the thinner overcast (see Eq. (1)). Best-fit equations are for the interval $380 \le \lambda \le 780$ nm, with proportionality constants $k_5 = 1.069$ and $k_6 = 2.544$.

by the best-fit power-law relationships $T(\lambda) \propto \lambda^{-0.611}$ for low T and $T(\lambda) \propto \lambda^{-0.270}$ for high T. A slightly more pronounced λ^{-c} dependence exists for stratocumulus overcasts (see Fig. 10). For example, at comparable T values in Figs. 9 and 10, c is ~44% larger for the stratocumulus overcasts. Thus at the same T or τ, a stratocumulus overcast will look slightly bluer than a stratus overcast. However, this distinction is often obscured for two reasons: (1) T is seldom equal in different overcasts (see Fig. 2), and (2) temporal color constancy[25] makes us less sensitive to any such daily changes in overcast color.

At wavelengths >550 nm, the measured $T(\lambda)$ spectra in Figs. 9 and 10 have local maxima and minima similar to those found in transmission spectra associated with continuum absorption by water vapor and oxygen.[26] Thus absorption by atmospheric gasses within clouds adds some spectral detail to overcast $T(\lambda)$ spectra, but it does not explain their λ^{-c} shape.

The fact that overcast $T(\lambda)$ varies approximately as λ^{-c} may be surprising, since this is also true of the Rayleigh blue sky, for which $L_\lambda \propto \lambda^{-4}$ (i.e., $c = 4$). Yet unlike the clear sky, in an overcast the amount of bluing *increases* with τ (i.e., with decreasing T). Thus thicker clouds are bluer. This strongly suggests that spectrally selective absorption rather than scattering ultimately causes the subtle bluing seen beneath overcasts.[27] In fact, we can use T to estimate overcast τ by modifying Bohren's two-stream radiative-transfer model[28] to include surface reflectance r. Then

$$\tau = \frac{2(T^{-1} - 1)}{(1 - r)(1 - g)}, \tag{2}$$

where g is the single-scattering asymmetry parameter for cloud droplets, and all variables are implicit functions of λ. Not surprisingly, Eq. (2) is most realistic for thicker overcasts where the assumptions of the two-stream model are best satisfied.

5. Modeling Overcast Transmission Spectra and Chromaticities

To analyze the fundamental optical properties that determine overcast $T(\lambda)$, we use the detailed and extensively tested radiative-transfer model MODTRAN4. MODTRAN combines features of horizontally homogeneous spherical-shell and plane-parallel atmospheres, and it calculates solar direct-beam and diffusely scattered components at each of the model's many vertical levels. Provided that $h_0 > 0°$, MODTRAN yields quite realistic L_λ and E_λ spectra for skylight and daylight.[29] Except as noted below, each of our MODTRAN simulations includes the following parameters: a default midlatitude winter atmospheric profile of temperature, pressure, humidity, and gas mixing ratios; tropospheric aerosols typical of rural sites; background stratospheric dust and other aerosols; multiple scattering; a Lambertian surface with $r = 0.2$ at all λ; and Mie aerosol phase functions.

In Fig. 11, we calculate MODTRAN's $T(\lambda)$ using downwelling surface E_λ for a stratus layer whose thickness $\Delta z = 670$ m and clear-sky E_λ at the same

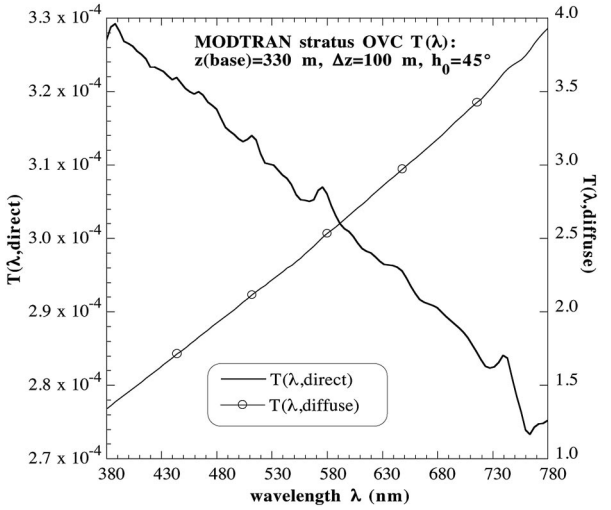

Fig. 12. Comparison of simulated MODTRAN $T(\lambda)$ for the direct-beam and diffuse components in Fig. 11's 100 m thick stratus overcast. $T(\lambda, \text{diffuse}) > 1$ because the diffuse irradiances at cloud bottom (the numerator in Eq. (1)) include energy scattered from the direct solar beam, whereas diffuse irradiances at cloud top exclude direct sunlight.

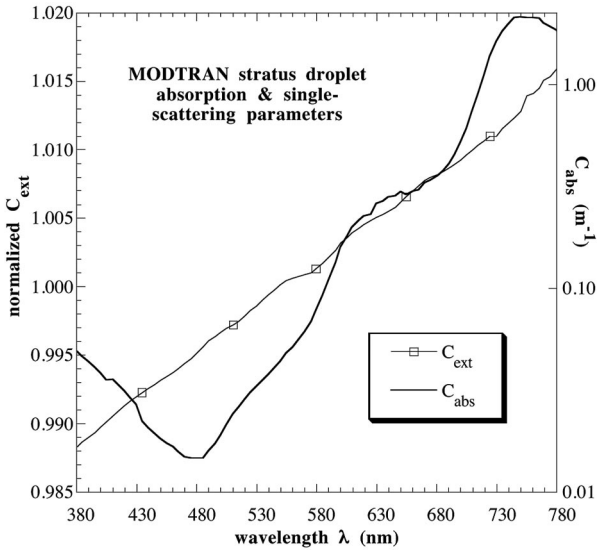

Fig. 13. MODTRAN visible-wavelength spectra of absorption cross section C_{abs} and extinction cross section C_{ext} for stratus droplets of radius a. C_{ext} is normalized by its value at 550 nm and is proportional to $2\pi a^2$. Note that C_{abs} is scaled logarithmically.

h_0. We also include in Fig. 11 a stratus overcast with $\Delta z = 100$ m, but here we calculate $T(\lambda)$ using simulated E_λ at cloud top and bottom. This change lets us examine in Fig. 12 the diffuse and direct-beam $T(\lambda)$ restricted to just the cloud itself. For the 100 m overcast in Fig. 11, mean T is naturally rather large, and $T(\lambda)$ is nearly spectrally neutral ($c = 0.065$). Yet unlike many other models, MODTRAN's simulated $T(\lambda)$ spectra closely resemble our measured $T(\lambda)$ spectra, including such features as continuum absorption by water vapor and oxygen. For example, compare the similar transmissivity curves $T(\lambda, 670\text{ m})$ in Fig. 11 and $T(\lambda, \text{high})$ in Fig. 9.

Figure 12 shows the very different MODTRAN $T(\lambda)$ spectra of daylight's attenuated direct-beam and amplified diffuse scattering components. Even a thin stratus overcast with $\Delta z = 100$ m nearly extinguishes the direct solar beam and makes it slightly bluer, as seen in the $T(\lambda, \text{direct})$ spectrum. Yet Fig. 12's $T(\lambda, \text{diffuse})$ spectrum is both >1 and redder at the cloud's bottom. This occurs because, by definition, the model's cloud-top diffuse E_λ consists only of energy from outside the Sun's solid angle. Thus it starts with a diffuse E_λ component predominated by blue skylight, but after traversing the cloud, this diffuse E_λ has (1) gained energy scattered from the direct beam, which (2) was much less blue than skylight to begin with, and from which (3) there is *slightly* preferential scattering of red light that adds to the diffuse downward E_λ.

In Fig. 13, we examine how absorption and extinction by stratus cloud droplets can account for MODTRAN's overcast colors. First, note that the size-dependent extinction for these relatively large (radius $a > 5$ μm) droplets is simply proportional to $2\pi a^2$. Second, MODTRAN's absorption coefficient for liquid water (C_{abs}) is significant only at $\lambda > 590$ nm, which apparently leads to droplets that have slightly nonneutral extinction cross sections C_{ext} at visible λ (C_{ext} increases ~2.7% from 380–780 nm).

So if extinction increases weakly with λ, then the (possibly) transmitted direct beam becomes *slightly* bluer, and the scattered light becomes *slightly* less blue, as we saw earlier. How do these droplet-level details help explain thick clouds' bluish color? Imagine an optically thick overcast with cloud normal $\tau > 100$. We routinely experience such overcasts, and as seen in Fig. 14, surface E beneath them decreases monotonically (but not linearly) with increasing Δz or

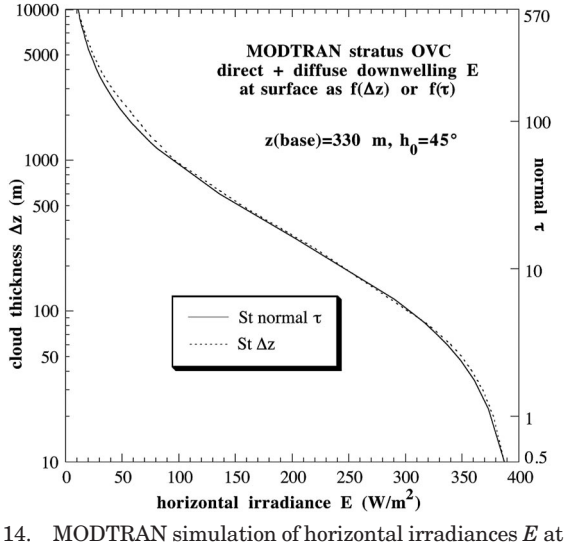

Fig. 14. MODTRAN simulation of horizontal irradiances E at the surface as a function of cloud thickness Δz. For normal optical depth τ, the $E(\tau)$ curve is not exactly congruent with the $E(\Delta z)$ curve because we calculate the former independent of MODTRAN using Eqs. (1) and (2).

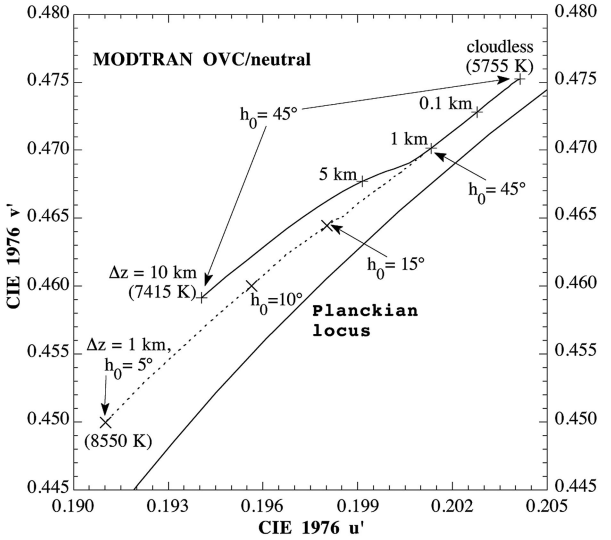

Fig. 15. MODTRAN simulations of stratus overcast u', v' chromaticities calculated from E_λ as functions of Δz and h_0. The dashed h_0 curve sets $\Delta z = 1$ km, and the solid Δz curve sets $h_0 = 45°$. The underlying Lambertian surface has a constant spectral reflectance $r_\lambda = 0.2$. During the daytime, simulated overcast colors grow steadily bluer as Δz increases and h_0 decreases.

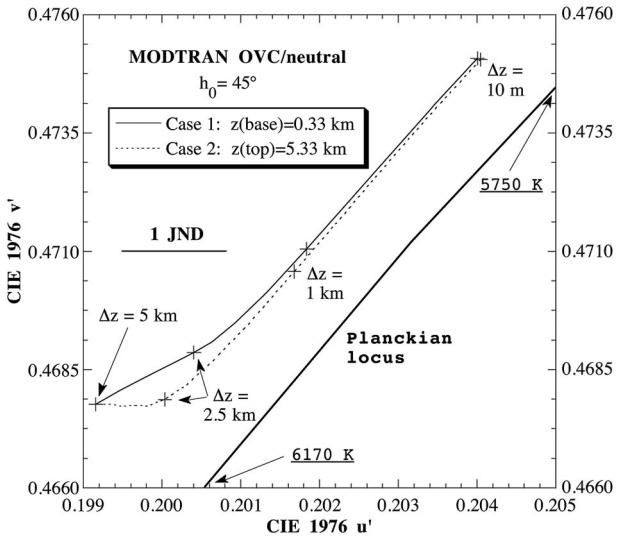

Fig. 16. MODTRAN simulations of stratus overcast u', v' chromaticities calculated from E_λ as functions of Δz for the cases of fixed-altitude tops z(top) and fixed-altitude bottoms z(base). Although the Case 2 chromaticities (fixed, high-altitude z(top)) are slightly bluer, in both cases bluing of daylight beneath the overcast depends much more strongly on cloud Δz.

τ. In Fig. 14, we use Eqs. (1) and (2) to calculate τ from MODTRAN overcast E.

Clearly in a neutrally absorbing, optically thick cloud, multiple scattering by large drops (i.e., $a \gg \lambda$) would only yield $T(\lambda)$ = constant. As in the popular misconception, light exiting such a cloud's bottom would have the same color as the daylight incident on its top. However, in real clouds with nonneutral C_{abs}, multiple scattering for large Δz or τ amplifies spectrally selective absorption enough to produce the clouds' bluish colors.[27] Because this bluing increases with cloud τ, absorption within water droplets and not droplet scattering in itself likely causes overcast colors. Multiple scattering also increases absorption by the increased amount of water vapor in and near the clouds, although this does not explain the overall λ^{-c} shape of $T(\lambda)$.

Now we use MODTRAN to help understand how overcast colors depend on h_0 and cloud Δz. In Fig. 15, MODTRAN's simulated stratus overcast colors become progressively bluer as Δz increases from 0 to 10 km, with CCT increasing by $\sim$1660 K for $h_0 = 45°$. For fixed $\Delta z = 1$ km, an even larger color shift occurs as h_0 decreases from 45° to 5° in Fig. 15. Unlike Fig. 6's observed local minimum in CCT near $h_0 \sim 30°$, MODTRAN predicts only a steady increase in CCT, with much of that increase occurring for $5° < h_0 < 10°$. In real overcasts, however, CCT can actually *decrease* with decreasing h_0 if Δz also decreases then (e.g., see the h_0 extremes in Fig. 1's Granada 11-8-03 chromaticity curve).

Might thick overcasts be bluish because their tops are illuminated by clear skylight whose blueness increases with altitude z? We know that skylight purity increases with z because multiple scattering in the clear atmosphere decreases with z.[30] Yet both a simple thought experiment and MODTRAN simulations show that cloud-top height z(top) contributes little to overcast bluing. Certainly downwelling clear-sky E_λ grow bluer as observer z increases, but only within limits. For example, we have measured daytime E_λ spectra at altitudes of $z \sim 3.8$ km that are distinctly bluer than those near sea level. However, this trend cannot continue indefinitely, since skylight radiances decrease with z even as their colorimetric purities increase. Ultimately, the purest blue skylight occurs at z such that only one molecule scatters sunlight to us; but then the sky will be black, not blue, and the color of daylight will be that of extraterrestrial sunlight.

In fact, blue skylight's increasing purity with z has only a minor effect on overcast colors at the surface. Depending on z(top), daylight incident on higher clouds may well be bluer than that on lower clouds, but the clear-sky molecular atmosphere still exists between the surface and z(top). Although the illumination geometry certainly changes for gas molecules within clouds, their spectral scattering properties are unchanged, and so will be their individual contributions to surface E_λ. MODTRAN simulations show that cloud thickness Δz plays a far more important role than z(top). In Fig. 16, we plot as functions of Δz the daylight chromaticities beneath two MODTRAN stratus overcasts for $h_0 = 45°$. These overcasts have either a fixed bottom z(base) = 0.33 km (Case 1) or a fixed z(top) = 5.33 km (Case 2); all other MODTRAN parameters are identical. As cloud Δz increases from right to left in Fig. 16, z(top) either increases (Case 1) or is constant (Case 2). Despite distinct differences in daylight spectra atop the Case 1 and Case 2 overcasts, they yield nearly identical chromaticity curves.

If daylight color beneath these two overcasts were

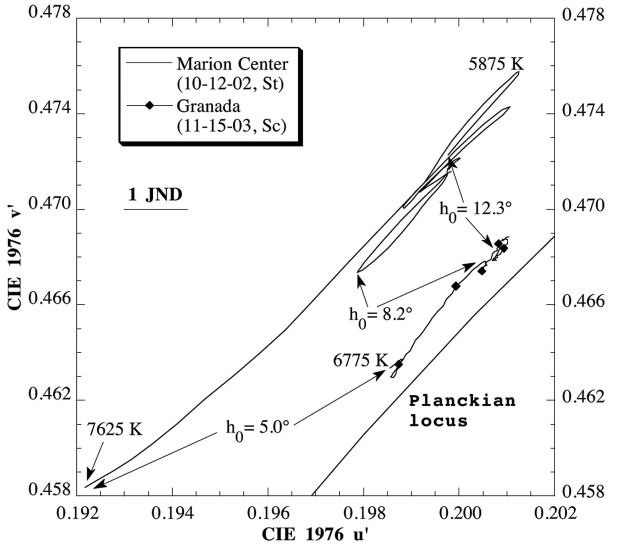

Fig. 17. Temporal trends in overcast u', v' chromaticities calculated from E_λ near Marion Center, Pennsylvania, on 10-12-02 and at Granada on 11-15-03; h_0 ranges from 5.0°–12.3°.

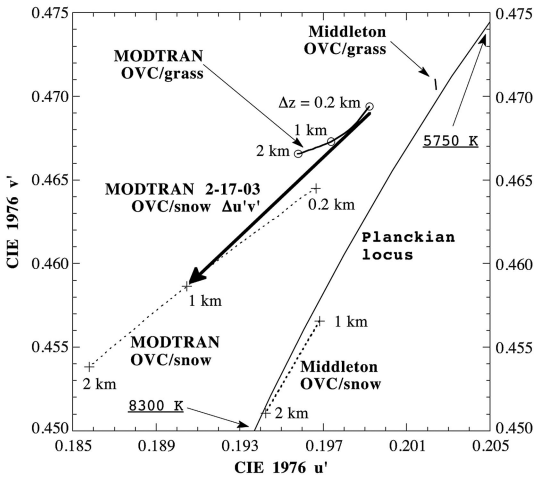

Fig. 18. MODTRAN simulations of stratus overcast u', v' chromaticities at the zenith as functions of cloud Δz and the underlying surface's spectral reflectance r_λ. The thick arrow indicates MODTRAN's prediction of the chromaticity shift caused by changing the surface from grass to snow for Fig. 19's observed changes in cloud Δz. For historical purposes, we also include overcast chromaticities simulated by Middleton.[4]

largely determined by z(top), then chromaticity distances $\Delta u'v'$ at the same Δz should be nearly as large as or larger than those caused by increasing cloud Δz (pairs of +'s in Fig. 16 mark equal-Δz chromaticities). Yet Fig. 16 clearly shows that this is not so: although Case 2 chromaticities are *slightly* bluer than those for Case 1 at the same Δz (i.e., Case 2 chromaticities are shifted slightly leftward), the maximum $\Delta u'v'$ at $\Delta z = 2.5$ km is *far less* than the $\Delta u'v'$ caused by a 2.5 km thick stratus overcast (i.e., the chromaticity distance between $\Delta z = 2.5$ km and $\Delta z = 10$ m). In particular, note that the largest Case 1–Case 2 color difference at $\Delta z = 2.5$ is still less than 1 JND. Similar results occur at smaller h_0. Thus multiple scattering and absorption within clouds, not the altitudes of cloud tops, chiefly determine daytime overcast colors at the surface.

In one sense, Fig. 17's measured chromaticities support MODTRAN's claim in Fig. 15 about the h_0-dependence of overcast colors: for both overcasts, the largest CCT increases occur at the smallest h_0. In Fig. 17, CCT increases steadily only when $h_0 < 8.2°$ (Granada 11-15-03) or $h_0 < 6.6°$ (Marion Center 10-12-02). However, the measured effects of cloud Δz seem to differ from those predicted by MODTRAN. Although the Granada overcast is consistently much darker than that at Marion Center (by an E factor $\sim$2.1), its mean u' is in fact larger, not smaller as MODTRAN predicts. Furthermore, MODTRAN predicts that the Granada chromaticity curve will shift rightward $\ll$1 JND as a result of Granada having a stratocumulus, rather than a stratus, overcast. Instead, Fig. 17's Granada curve >1 JND to the right of the Marion Center curve. Our point here is not that MODTRAN is unrealistic but that ultimately we must know more about overcast illumination and internal structure (e.g., clouds at other z, vertical inhomogeneities in droplet and haze number densities, detailed drop size distributions) before we can test the model rigorously.

6. Overcast Color and Surface Color

Some 50 years ago, Middleton made one of the first systematic attempts to predict overcast sky colors. He did so by incorporating spectral ground reflectance r_λ and scattering and absorption by cloud droplets into a model of overcast spectra in a plane-parallel atmosphere. Other model parameters included cloud thickness, droplet number density, and monodisperse droplet radius and scattering coefficient; h_0 was fixed at 23°. When Middleton ultimately calculated chromaticities from E_λ beneath the overcast, he decided to ignore absorption by both droplets *and* their inclusions, asserting that the overcast sky's chromaticity and luminance are to "a considerable extent a function of the reflectance of the ground, but depend only to a minor degree on the presence of dissolved absorbing matter in the cloud water."[4] As beneficiaries of several additional decades of research on overcasts, what new can we say about Middleton's claims?

In Fig. 18, the short line segment at upper right connects Middleton's predicted chromaticities for overcasts with cloud $\Delta z = 1$ km or 2 km above grass. A longer line at Fig. 18's bottom connects his chromaticities for the same Δz pair above snow. Middleton thus predicts that the same overcast will be markedly bluer above snow than above grass. Although MODTRAN makes the same qualitative prediction about snow's effect, quantitatively it greatly expands Middleton's overcast $\hat{g}$ for overcast/grass and shifts those chromaticities toward higher CCT. Given that both models use similar r_λ spectra for grass and for snow, their differences probably are not caused by the underlying surfaces.

Because snow reflects more bluish cloud light to the

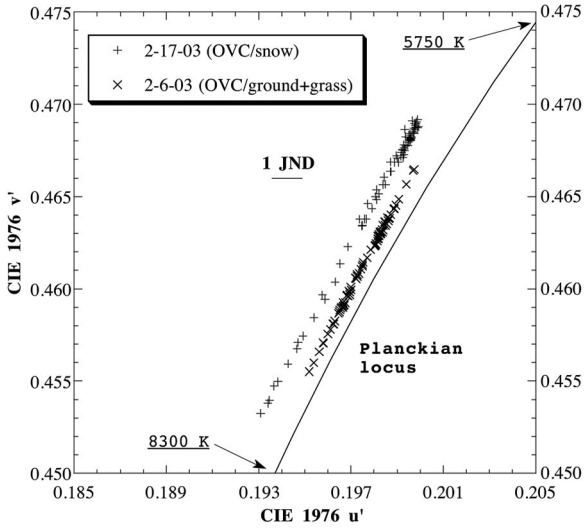

Fig. 19. Scatterplot of overcast u', v' chromaticities calculated from zenith L_λ at Owings during stratus overcasts on 2-6-03 and 2-17-03; h_0 ranges from 14.4°–20.5°. Only on 2-17-03 was the ground snow-covered. Compare these measured chromaticities with MODTRAN simulations in Fig. 18.

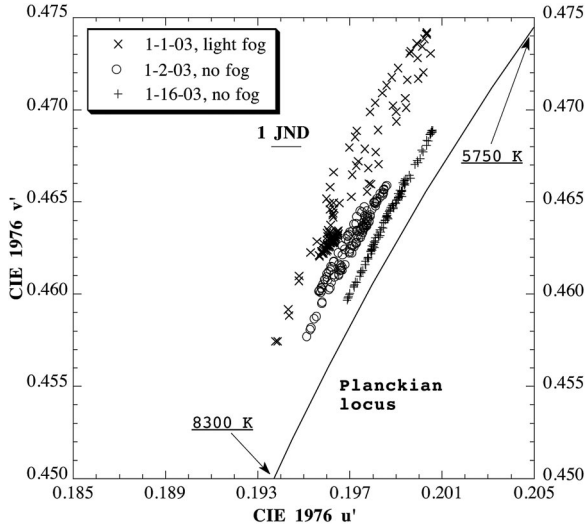

Fig. 20. Scatterplot of overcast u', v' chromaticities calculated from zenith L_λ at Owings during stratus overcasts on 1-1-03, 1-2-03, and 1-16-03. The ground was snow-free on all days; h_0 ranges from 12.3°–20.2°.

cloud's bottom than does grass (i.e., the cloud bottom is brighter above snow), there is more scattering within the cloud. More germane for us is that the additional scattering results in additional spectrally selective *absorption* by the cloud. Some of the remaining blue-enhanced light is then scattered downward to our eyes and radiometers, making the overcast both bluer and brighter than it would be over a low-r surface. In effect, snow increases overcast blueness by increasing cloud Δz and τ.

Middleton's chromaticities for an overcast above snow clearly are incorrect because they are on the opposite side of the Planckian locus from our measured chromaticities. This problem may be caused by Middleton's decision to ignore spectral absorption by cloud water. Yet MODTRAN avoids this problem above snow cover only to encounter others. In Fig. 19, the 2-17-03 overcast immediately followed a major winter storm that left ~0.3 m of snow on the ground at Owings; on 2-6-03 the ground was snow-free. On both days, nearly featureless stratus clouds comprised the overcast. The most obvious colorimetric differences between Fig. 19's two overcasts are that the post-snow $\hat{g}$ increases in size and shifts slightly leftward. This observed behavior is quite different from that of MODTRAN,[31] which predicts large shifts away from the Planckian locus and toward higher CCTs (see Fig. 18's thick arrow).

In fact, surface r_λ may matter less than either Middleton's model or MODTRAN suggest. Using the same u', v' scale as Figs. 18 and 19, Fig. 20 shows overcast zenith chromaticities measured at Owings on three snow-free days in January 2003. Although the surface r_λ changed little during this two-week period, the spread in Fig. 20's overcast chromaticities is comparable to that in Fig. 19. Furthermore, the 1-1-03 overcast has many chromaticities that are displaced even farther from the Planckian locus than are Fig. 19's most distant post-snow colors. This observation naturally raises the question of how much of Fig. 19's chromaticity shift is due to snow. To us, Figs. 19 and 20 suggest that daily (and even minute-by-minute) changes in cloud τ_λ may well do more to affect overcast colors than all but the most extreme shifts in surface r_λ.

7. Conclusions

Our measurements of overcast $T(\lambda)$ spectra (Figs. 9 and 10) should help dispel any lingering notion that overcasts are spectrally neutral transmitters of visible-wavelength daylight. While overcast colors literally pale in comparison to their spectacular cerulean counterparts, they have much to teach us about radiative transfer in clouds. Although the total depth of liquid water in even the thickest overcast is quite small, multiple scattering greatly enhances the small amount of spectrally selective absorption that occurs each time light interacts with a cloud droplet.[28] After many scatterings, the amount of bluing caused by thick clouds is quite perceptible, as even a casual inspection of their bottoms reveals (Fig. 5). Continuum absorption by water vapor and oxygen adds important spectral details at longer visible wavelengths in $T(\lambda)$ spectra (Figs. 9 and 10),[26] but does not explain their overall shape or the resulting overcast colors.

However drab the colors of overcast skies may seem visually, explaining their chromaticities and (ir)radiance spectra continues to be a challenge. First, the observed $\hat{g}$ of daylight from overcasts usually is larger than that of clear-sky daylight (Fig. 1), and MODTRAN simulations only begin to mimic this range of colors (Figs. 15 and 18). Second, sorting out the relative spectral contributions of overcasts' $T(\lambda)$ or τ_λ, the E_λ spectra incident on the clouds' tops, and the r_λ spectra of the underlying surface remains dif-

ficult many years after Middleton's pioneering work. Our research suggests that r_λ probably is less important than he concluded, and that other purely atmospheric factors such as the presence of fog (see Fig. 20's 1-1-03 overcast) are more important. Finally, overcasts' apparent visual simplicity hides great colorimetric and spectral complexity. To understand this complexity better, in future research we will consider vertical and horizontal inhomogeneities within optically thick clouds. Thus while overcast colors may look pedestrian, they offer a wealth of new insights in atmospheric optics.

Several agencies generously funded this research. Lee was supported by United States National Science Foundation grant ATM-0207516 and by the United States Naval Academy's Departments of Physics and Mathematics. Hernández-Andrés was supported by Spain's Comisión Interministerial de Ciencia y Tecnología (CICYT) under research grant DPI2004-03734.

References and Notes

1. B. A. Kimball, S. B. Idso, and J. K. Aase, "A model of thermal radiation from partly cloudy and overcast skies," Water Resour. Res. **18,** 931–936 (1982).
2. Harshvardhan, W. Ridgway, V. Ramaswamy, S. M. Freidenreich, and M. Batey, "Spectral characteristics of solar near-infrared absorption in cloudy atmospheres," J. Geophys. Res. **103,** 28793–28799 (1998).
3. C. Erlick, J. E. Frederick, V. K. Saxena, and B. N. Wenny, "Atmospheric transmission in the ultraviolet and visible: aerosols in cloudy atmospheres," J. Geophys. Res. **103,** 31541–31555 (1998).
4. W. E. K. Middleton, "The color of the overcast sky," J. Opt. Soc. Am. **44,** 793–798 (1954).
5. V. Hisdal, "Spectral distribution of global and diffuse solar radiation in Ny-Ålesund, Spitsbergen," Polar Res. **5,** 1–27 (1987).
6. J. Hernández-Andrés, R. L. Lee, Jr., J. Romero, and J. L. Nieves, "Color and spectral analysis of daylight in southern Europe," J. Opt. Soc. Am. A **18,** 1325–1335 (2001).
7. E. M. Feigelson, *Radiation in a Cloudy Atmosphere* (Reidel, Dordrecht, 1984), pp. 52–62, 164–169.
8. S. Nann and C. Riordan, "Solar spectral irradiance under clear and cloudy skies: measurements and a semiempirical model," J. Appl. Meteorol. **30,** 447–462 (1991).
9. D. A. Siegel, T. K. Westberry, and J. C. Ohlmann, "Cloud color and ocean radiant heating," J. Climate **12,** 1101–1116 (1999).
10. *Spatial Distribution of Daylight—CIE Standard Overcast Sky and Clear Sky*, CIE Standard S 003/E-1996 (Commission Internationale de l'Eclairage, Vienna, 1996), p. 3.
11. G. Wyszecki and W. S. Stiles, *Color Science: Concepts and Methods, Quantitative Data and Formulae*, 2nd ed. (Wiley, New York, 1982), pp. 144–145.
12. Sometimes this spectral assumption is explicit, as in A. J. Preetham, P. Shirley, and B. Smits, "A practical analytic model for daylight," in *SIGGRAPH 99 Conference Proceedings*, A. Rockwood, ed. (Association for Computing Machinery, New York, 1999), pp. 91–100.
13. T. S. Glickman, ed., *Glossary of Meteorology,* 2nd ed. (American Meteorological Society, Boston, 2000), p. 550.
14. Although the CIE 1976 UCS diagram is itself perceptually isotropic, note that in order to show as much detail as possible, we make the ordinate and abscissa scales differ in Fig. 1 and later chromaticity diagrams.
15. PR-650 spectroradiometer from Photo Research, Inc., 9731 Topanga Canyon Place, Chatsworth, Calif. 91311. According to Photo Research, at specified radiance levels a properly calibrated PR-650 measures luminance and radiance accurate to within $\pm 4\%$, has a spectral accuracy of ± 2 nm, and its CIE 1931 colorimetric errors are $x < 0.001$, $y < 0.001$ for a 2856 K blackbody (CIE standard illuminant A).
16. R. L. Lee, Jr., "Twilight and daytime colors of the clear sky," Appl. Opt. **33,** 4629–4638, 4959 (1994). Gamut $\hat{g}$ ranges from 0 for constant chromaticity to 1 for the spectrum locus, and thus represents the fraction of the CIE diagram that a given chromaticity curve spans.
17. R. L. Lee, Jr. and J. Hernández-Andrés, "Measuring and modeling twilight's purple light," Appl. Opt. **42,** 445–457 (2003).
18. Reference 11, pp. 306–310.
19. Reference 11, pp. 306–310. Here we follow convention and set the JND equal to the semimajor axis length of the MacAdam color-matching ellipse at the given chromaticity.
20. D. B. Judd, D. L. MacAdam, and G. Wyszecki, "Spectral distribution of typical daylight as a function of correlated color temperature," J. Opt. Soc. Am. **54,** 1031–1040 (1964).
21. J. Hernández-Andrés, R. L. Lee, Jr., and J. Romero, "Calculating correlated color temperatures across the entire gamut of daylight and skylight chromaticities," Appl. Opt. **38,** 5703–5709 (1999).
22. *Olympus Camedia E-10 User's Manual* (Olympus Optical Co., Ltd., Tokyo, 2000), p. 102.
23. Reference 11, pp. 224–225.
24. Our experience is that cloud tops occur approximately where radiosonde relative humidity falls below 96% as altitude z increases. Using this admittedly imperfect criterion, for 24 different overcasts our mean cloud-top $z(\text{top}) = 1700$ m above sea level, median $z(\text{top}) = 1445$ m, and the $z(\text{top})$ standard deviation = 961 m.
25. R. Sekuler and R. Blake, *Perception* (Knopf, New York, 1985), pp. 189–192.
26. B. Sierk, S. Solomon, J. S. Daniel, R. W. Portmann, S. I. Gutman, A. O. Langford, C. S. Eubank, E. G. Dutton, and K. H. Holub, "Field measurements of water vapor continuum absorption in the visible and near-infrared," J. Geophys. Res. **109 (part 8),** D08307 (2004).
27. C. F. Bohren and A. B. Fraser, "Green thunderstorms," Bull. Am. Meteorol. Soc. **74,** 2185–2193 (1993).
28. C. F. Bohren, "Multiple scattering of light and some of its observable consequences," Am. J. Phys. **55,** 524–533 (1987). Our Eq. (2) is derived from Bohren's Eq. (15) for T as a function of τ, and we use Bohren's value of $g = 0.85$ for visible-wavelength scattering by cloud droplets.
29. MODTRAN uses a plane-parallel atmosphere to calculate multiple-scattering contributions to daylight and skylight, and when $h_0 \leq 0°$ the model produces nonphysical spectra in the visible.
30. C. F. Bohren and A. B. Fraser, "Colors of the sky," Phys. Teach. **23,** 267–272 (1985).
31. Based on radiosonde data from nearby Dulles International Airport (code IAD), we estimated cloud $\Delta z = 0.2$ km and 1.0 km on 2-6-03 and 2-17-03, respectively. Perhaps surprisingly, using r_λ for green grass in the 2-6-03 wintertime landscape was not unrealistic (this choice aids comparison with Middleton's results in Fig. 18). Even though we do not know the actual mean Owings r_λ spectrum on 2-6-03, MODTRAN predicted negligible differences in overcast chromaticities when we tried several different materials (e.g., tree bark, a mixture of dead and living vegetation) for the snow-free surface's r_λ.